

RSC Advances



This is an *Accepted Manuscript*, which has been through the Royal Society of Chemistry peer review process and has been accepted for publication.

Accepted Manuscripts are published online shortly after acceptance, before technical editing, formatting and proof reading. Using this free service, authors can make their results available to the community, in citable form, before we publish the edited article. This *Accepted Manuscript* will be replaced by the edited, formatted and paginated article as soon as this is available.

You can find more information about *Accepted Manuscripts* in the [Information for Authors](#).

Please note that technical editing may introduce minor changes to the text and/or graphics, which may alter content. The journal's standard [Terms & Conditions](#) and the [Ethical guidelines](#) still apply. In no event shall the Royal Society of Chemistry be held responsible for any errors or omissions in this *Accepted Manuscript* or any consequences arising from the use of any information it contains.

Going Beyond The Self-Assembled Monolayer: Metal Intercalated Dithiol Multilayers and Their Conductance.

Hicham Hamoudi^{1*}, Kohei Uosaki¹, Katsuhiko Ariga¹, Vladimir A. Esaulov²

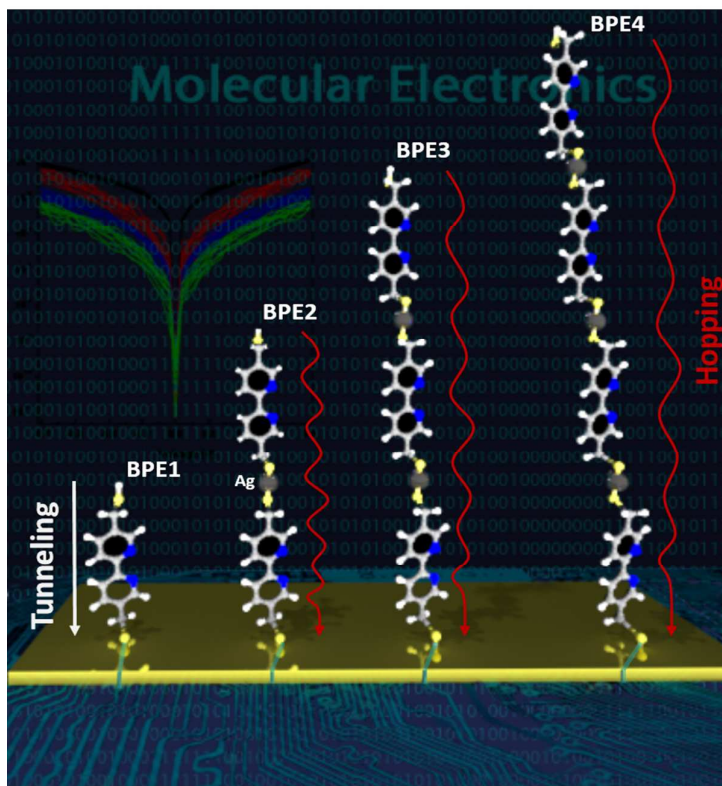
¹*International Center for Materials Nanoarchitectonics (WPI- MANA), National Institute for Materials Science (NIMS), 1-1 Namiki, Tsukuba, 305-0044, Japan.*

²*Institut des Sciences Moléculaires d'Orsay, Unité mixte de Recherche CNRS- Université Paris Sud, UMR 8214, bât. 351, Université Paris Sud, Orsay 91405, France*

Abstract:

A study of the self-assembly of silver atom intercalated 5,5'-Bis(mercaptomethyl)-2,2'-bipyridine (BPD; HS-CH₂-(C₅H₃N)₂-CH₂-SH) and 1,4-benzenedimethanethiol (BDMT; HS-CH₂-(C₆H₄)-CH₂-SH) dithiol (DT) multilayers on gold is presented. The bilayer of these SAMs can be obtained starting from the exposure of a DT monolayer to a concentrated silver ion solution. After grafting the silver atoms on the sulfur end group, the incubation of the resulting DT-Ag SAM in a DT solution leads to the formation of a DT-Ag-DT bilayer. This process was extended to make a multilayer structure. The corresponding changes in these self-assembled layers on Au are characterized by X-ray photoelectron spectroscopy (XPS), spectroscopic ellipsometry (SE) measurements, and *I-V* characteristic. Our interpretation of evolution in the absorbed layer are based on changes in intensities of peaks in XPS related to S bound to substrate or Ag and in -SH groups, as well as changes in thickness and absorption features in SE measurements. The latter show the evolution in absorbance wavelength as a function of thickness and indicate a decrease in HOMO-LUMO gap from about 4.5eV to 4eV. The *I-V* characteristics show a significant bias dependence to the number of the BPD layers and there appears to be a transition in from tunneling to a hopping regime when going from the single to the multiple layers.

Corresponding authors: H. Hamoudi: Phone: +81-29-851-3354 (ext.8672), FAX: +81-29-860-4706, E-mail: HAMOUDI.Hicham@nims.go.



TOC Figure

Introduction

In this paper we address the question of step by step building up of organic-metal-organic heterostructures. Metallization of organic layers^{1,2} is a subject of longstanding interest and many applications can be found in every-day-life. This subject has attracted much attention recently because of interest in organic electronics, light emitting diodes, sensors and in general in relation with adhesion of bio-molecules to surfaces, with e.g. applications in biology and medicine. A step beyond this is building up of more complex organic-metal-organic scaffolds.

The basic building block in our work is a dithiol molecule, which provides the possibility of using the two-thiol terminations to bind to different metallic entities.¹⁻⁶ Thus in some earlier works eg pentanedithiol molecules were used⁴ to first assemble a SAM on a metal surface from ethanolic solutions, then deposit on them metal nanoparticles and finally upon these graft further pentanedithiols. Similar attempts have been made and by some of us^{7, 47, 48, 49} e.g. using 1,4-benzenedimethanethiol (BDMT) and hexanedithiol SAMs prepared in ethanolic solutions, with electrochemical deposition of metal atoms on the SAM.

It should be noted that interest in molecules with phenyl units is related to the fact that they have better conducting properties and are better adapted as molecular contacts between nanosized metallic electrodes.⁷⁻¹⁸ Indeed, the first conduction measurements on molecules involved measuring the resistance of a 1,4-benzenedimethanethiol (BDMT) molecule.¹⁹ This was performed using a scanning tunneling microscopy (STM) tip held on a gold nanoparticle deposited on top of a BDMT SAM. Thus the case of BDMT molecules presented a particular interest for these studies. It is worth noting here that generally molecules do not behave as simple ohmic conductors and have non-linear current-voltage characteristics. The problem of conductivity in molecular weirs have been a subject of different investigations.^{41, 42} Recently the electrical resistance of oligophenyleneimine (OPI) molecules of various lengths have been investigated using a conductive AFM tip.⁴² Hopping transport was found in longer OPI molecules, while the small molecules in length exhibited coherent transport. Similar results have been reported using the Fe(II)-bis(terpyridine) molecular system.⁴¹

In practice, the formation of a highly ordered compact SAMs, with free -SH end groups at the outer interface, depends on various factors such as the quality of the substrate and reagents, solvent strength, photochemical action, and so on, and has been, and is still debated. Thus for instance, solution formation of small length alkane SAMs, like the pentanedithiol and hexanedithiol SAM mentioned above^{4,7}, is known to be problematic and frequently leads to mainly lying down molecules.^{20,21,22} Similarly we have observed previously^{23,24} that assembly of BDMT in ethanolic solutions as used in⁷ is problematic and can lead to disordered layers. Thus the first step in building such organic metal organic heterostructures requires the establishment of robust standing up ordered dithiol SAM formation protocols. We recently investigated assembly of several alkanedithiol and also BDMT dithiol molecules²⁰⁻²⁷ using a combination of different techniques. SAMs based on BDMT grown on noble metals from solution were chosen as a good prototype system for the study of aromatic dithiol assembly (DT). The assembly of these molecules shows a better stability compared to saturated molecules because of the lateral interactions between the aromatic rings of adjacent molecules. We found previously that dithiol SAMs with aromatic units are better ordered than the ones with CH₂ groups.²¹⁻²⁴ A well reproducible protocol, allowing formation of well-ordered BDMT SAMs from degassed n-hexane solutions, in the absence of light, was established^{23, 24, 50} and the SAMs characterized by high resolution XPS, NEXAFS, RAIRS and spectroscopic ellipsometry (SE). These studies thus showed formation of an ordered SAM with standing up DT molecules inclined at 24° to the normal.

Layer by layer assembly starting from a SAM, has attracted much interest⁵¹ and different approaches depending upon molecule type have been attempted⁵²⁻⁵⁴. Here we ask ourselves the question whether it is indeed possible to build a multilayer SAM starting from the highly quality dithiol SAM? We base ourselves on the results of these earlier works^{23, 24, 50}, and have used a combination of SE, and XPS to study the formation of the bilayer of BDMT and also 5,5'-Bis(mercaptomethyl)-2,2'-bipyridine (BPD) self-assembled films on Au, with intercalated Ag atoms. In the following we refer to these generically as DT (dithiols). As shall be described below, first a DT SAM has been prepared using our established protocol. Then silver atoms were grafted to the SH end groups in a silver nitrate solution. We thus obtained a

platform for further deposition of DT leading to a DT-Ag-DT bilayer on gold as schematized in fig.1. This process is further repeated to obtain longer molecular chains of up to four DT units. The conduction through these was then investigated to study differences as a function of chain length and strong differences were found when going from a SAM to the multilayers. In the following we shall refer to these scaffolds by the number of DT units as DT_n (or BPD_n).

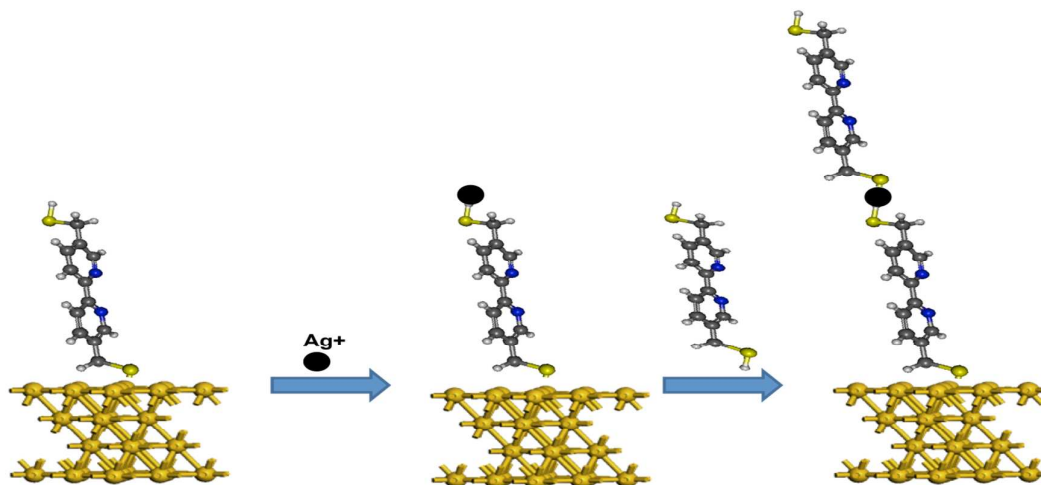


Figure 1. Schematics of the method to prepare a BPD-Ag-BPD layer, we use in this paper.

Experimental Section.

BDMT (98% purity) and BPD(96% purity) were purchased from Aldrich and used as received. The gold substrates were prepared by thermal evaporation of 150 nm of gold (99.99% purity) onto either polished single-crystal silicon (100) wafers primed with a 10 nm titanium adhesion layer or on freshly cleaved mica at 340 °C. The DT SAM was prepared by immersing the gold support into a freshly prepared 1mM solution of n-hexane. We used solutions well-degassed by Ar, and all preparation steps were performed, following the same protocol as in our previous studies.^{20,23} After that the gold wafer, modified with a layer of DT, was held in contact with 10 mM of AgNO₃

for 10 min at ~ 60 °C. Finally the resulting DT-Ag SAM was incubated in the DT solution as in the first step to yield the DT-Ag-DT bilayer. This procedure was extended to yield tri and quad layer Ag intercalated DT SAMs.

XPS spectroscopy measurements were conducted at the MANA Foundry using the XPS Thermo Fisher (Alpha 110 mm Analyser Sigma XPS version). The XPS spectra were recorded in the Au 4f, S 2p, and C 1s, and N 1s regions. The spectra acquisition was performed in normal emission geometry using the Al $K\alpha$ radiation. The binding energy (BE) scale of each spectrum was individually calibrated to the Au 4f_{7/2} emission at 83.95 eV.

SE measurements were performed in the MANA Foundry on a recently upgraded rotating compensator spectroscopic ellipsometer (M-2000, J.A. Woollam Co. Inc.). The experimental protocol adopted for SE measurements on ultrathin layers has been thoroughly described in recent articles on thiolate SAMs on gold.²⁸⁻³⁰ The rather small spectral variations induced by the formation of nanometer thick layers are best seen by calculating the difference between the data for pristine and SAM covered substrates ($\delta\Psi = \Psi_{\text{film}} - \Psi_{\text{Au}}$, $\delta\Delta = \Delta_{\text{film}} - \Delta_{\text{Au}}$), for several zones of each sample. In this work spectra have been collected at 65° and 70° angles of incidence. The spot size on the sample was of the order of a few square millimeters. Measurements were performed *ex situ*, in laboratory atmosphere, immediately after extraction from solution and adequate rinsing.

The mono and the multilayers junctions were electrically tested on a probe station using a semiconductor parameter analyzer (Keithley Instruments Inc.) at room temperature and under vacuum to avoid the influence of water.

Results

XPS measurements

The SAM for BDMT/Au and BPD/Au were investigated by XPS. Here we will focus on the BPD based system, while some BDMT based data is given in the supplementary information (fig.S1). Figure 2a shows the S2p and the C1s peaks regions of a BPD-Au sample, which was prepared by immersing in a freshly prepared, degassed, 1 mM solution of n-hexane for 1h at ~ 60 °C.

The C 1s spectra of the BPD, are presented in Figure 2b, with a decomposition into two components. The main peak at about 284.9 eV of the BPD SAM is a superposition of contributions from: the C-C moieties, and the C=C in the ring unit,^{24,31} while the 285.6eV peak is assigned to C-N.

The S(2p) spectra are decomposed into two components: two doublets with a fine structure splitting of 1,18eV corresponding to S atoms bound to gold (S_{Au} at 162 eV) and “free” S_H atoms on top of the BPD SAM (at 163,5 eV). The initial BPD spectrum resembles the one measured for BDMT here (fig.S1) and reported previously²³, but has different relative intensities of the S_{Au} and S components. We recall that the S_{Au} component appears with a lower intensity, because of attenuation of intensity of electrons passing through the organic layer^{23,24}. Because the BPD molecules are longer they result in a greater attenuation of electrons passing through the thicker layer and the S_{Au} intensity is lower than for BDMT. We shall return to this point later.

Oxygen-coordinated sulfur species are practically absent since no peaks with S ($2p_{3/2}$) binding energies above 168 eV are detected. The N 1s XPS spectra of the BPD SAM are displayed in Figure 3. A single symmetric peak at 399 eV is observed and assigned to the nitrogen in the pyridine rings.

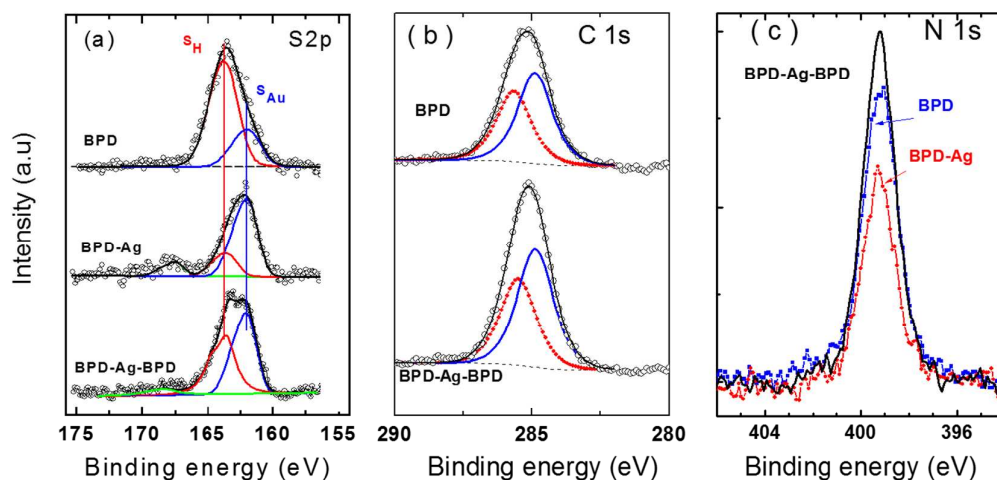


Figure 2. *S2p*, *C1s* and *N1s* XPS spectra of BPD, BPD-Ag, and BPD-Ag-BPD

Upon immersion of the DT SAM on Au, into the $AgNO_3$ solution the ratio of the S_{Au} and S_H components changes and the S_{Au} component increases significantly after exposure to Ag, as shown for the BPD case in fig2a. We ascribe this to binding of Ag atoms to the top sulfur S_H atoms, thus leading to a shift to lower core level binding energies, corresponding to binding to Ag, that is similar to the Au one³². This results in

the increase of the S_{Au} peak intensity. In the present experiments, a small amount of the 163 eV S component remained.

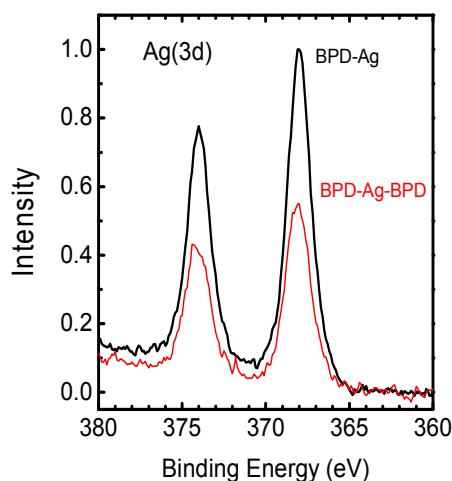


Figure 3. Ag 3d XPS spectra of the BPD-Ag and BPD-Ag-BPD layers.

The XPS investigation shows that Ag is indeed attached to the SAM, since we observe (fig.3) peaks at 368 eV and 373.9 eV, corresponding to the $Ag3d_{3/2}$ and $Ag3d_{5/2}$.³² This Ag spectrum appears quite symmetric and thus suggests a metallic nature of the deposit.³²

The Ag-DT SAMs on Au were re-immersed into the n-hexane DT solution using the same protocol. The resulting XPS spectrum is shown in Figure 2a for BPD. In this case we see a re-increase of the “free” S component, which we ascribe to binding of BPD molecules on top of the Ag-BPD SAM, and the resulting layer thus has free sulfur on top. Again the oxidized S structure appears to be quite small.

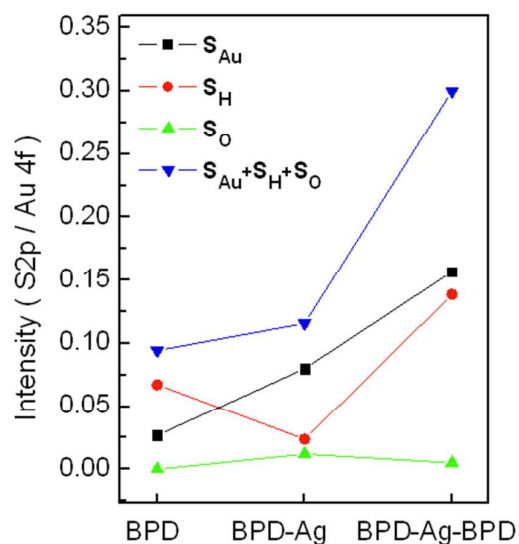


Figure 4: The intensity ratio S_{2p} to $Au\ 4f$ for the BPD, BPD-Ag and BPD-Ag-BPD layers.

The total integrated intensity of the S_{Au} and S_H related peaks of the BPD, BPD-Ag and BPD-Ag-BPD SAM is shown in fig.4. One can clearly see here the decrease in the S_H component for the BPD-Ag SAM and its re-increase in case of the BPD-Ag-BPD layer.

The Ag 3d peak intensity now decreases in the case of the BPD-Ag-BPD SAM, because of the screening of Ag by the BPD molecules attached to the Ag atoms on top of the BPD-Ag SAM (see figure 3).

We also observed (fig.2c) that the N(1s) intensity decreased for the BPD-Ag case, as could be expected because of additional Ag induced screening and then increased again for the BPD-Ag-BPD case, because of appearance of the second BPD layer.

The XPS data were additionally used to determine the effective thickness of the different SAMs (DT-Ag, and DT-Ag-DT). This was done on the basis of the Au 4f intensity, assuming a standard exponential attenuation of the photoelectron signal and using the attenuation lengths reported in ³¹. Calculating the film thickness from the C1s and Au4f signals values of ~ 1.95 and ~ 4.1 nm are obtained for BPD-Ag and BPD-Ag-BPD, respectively.

A more detailed analysis of changes in the S 2p XPS spectral shapes and some comments about intensity changes shown above are discussed in greater length in a following section.

Spectroscopic ellipsometry.

SE measurements were performed on the various layers studied. Results for BDMT SAM are given in the supplementary information (fig.S4). Data for BPD are shown in Figure 5a,b. For comparison we also performed measurements for an octadecane thiol (C18). The data are shown in the 245-1000 nm range for a 65° angle of incidence. The shapes of BPD $\delta\Psi$ and $\delta\Delta$ spectra resemble the ones for BDMT measured here and reported previously²³ using the same preparation method. The $\delta\Psi$ BPD curve shows a dip for wavelengths less than 350 nm (minimum around 275nm), a behavior similar to the BDMT case, for which it was previously²³ assigned to absorption, related to aromatic rings, eventually influenced by intermolecular interactions in the SAM²³. We performed a measurement of absorption on a sample of BPD solution in water (in which BPD is more easily soluble than in hexane), which indeed shows absorption below 325nm wavelength range (first peak at 293nm; see inset in fig.5). Given solvent related shifts in absorption features and the fact that we deal with a SAM we believe our interpretation is reasonable.

We also observe, as reported earlier for thiolate SAMs and BDMT, that for wavelengths above about 550nm, the $\delta\Psi$ curve has a negative value. This phenomenon has been interpreted as due to the formation of a strong molecule-surface bond, leading to charge redistribution and chemisorption-induced structural and morphological changes which affect the mean free path of electrons^{23, 28, 30}

A comparison of the $\delta\Psi$ and $\delta\Delta$ spectra for the BDMT and BPD SAMs shows larger positive and negative values of $\delta\Psi$ and $\delta\Delta$ respectively for the BPD case in agreement with the longer length of the BPD molecule ~ 2 nm. These data are directly compared with $\delta\Delta$ spectra obtained for C18 SAMs deposited under the same conditions of substrate preparation and incubation in order to estimate the thickness of the layer. The results for C18 are compatible with earlier work.^{29, 30} We see that the results for the C18 SAM and BPD-Ag SAM are fairly close, indicating that they have similar thickness. Thickness simulations in earlier works give a layer thickness of about 2.5

nm³⁰ for a C18 SAM is slightly higher than our estimate for BPD from XPS.

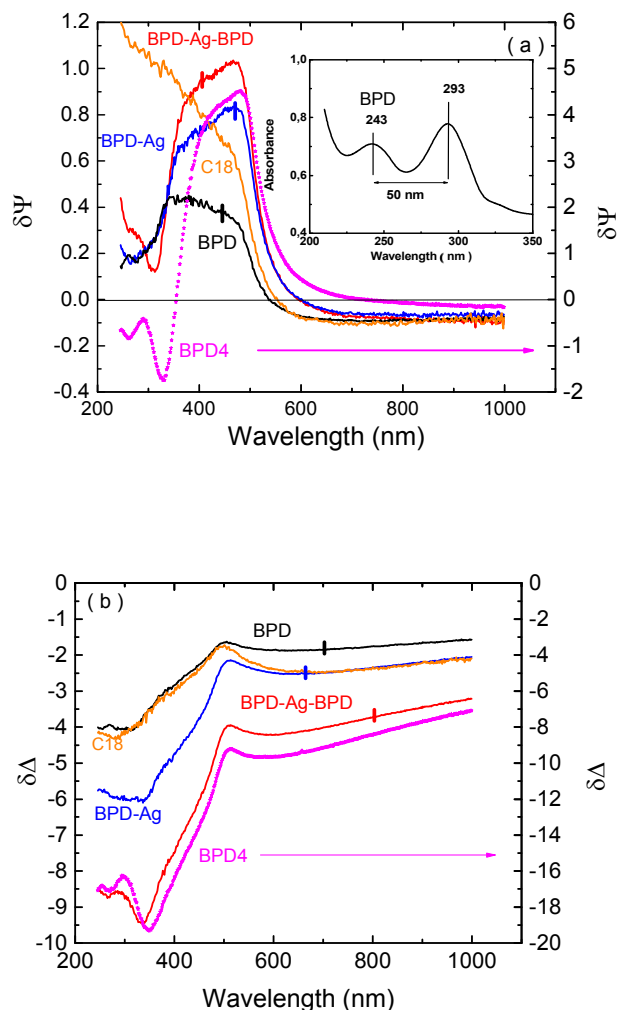


Figure 5: SE measurements for the BPD, BPD-Ag, BPD-Ag-BPD and BPD4 layers: (a) $\delta\Psi$ and (b) $\delta\Delta$. Note that the BPD4 data refers to the scale at the right. Data for C18 SH SAM is shown for comparison.

Upon immersion into the AgNO_3 solution, one can observe an increase in the $\delta\Psi$ curve values for wavelengths lower than 600nm, which can be related to an increase in thickness due to top Ag atoms. An interesting feature here is that there is now a decrease in $\delta\Psi$ curve for wavelengths lower than 480 nm. It is well known that Ag nanoparticles display a strong plasmon absorption peak, which, depending on size^{33,34}, is located in the 400 to 500nm range. Also absorption for Ag molecules, studied e.g. in

matrices is observed in the 300nm to 400nm range depending on the number of atoms.³⁵ We note that in a different system (titanosilicate) aggregation of isolated Ag⁺ ions into metal nanoclusters of increasing nuclearity was observed³⁶ to lead to absorption in this wavelength range. The nucleation of ions into clusters may be accompanied by charge transfer and neutralization through the molecular layer. One can thus tentatively assign this decrease in our $\delta\Psi$ curve to the formation of the Ag layer on top of the BPD SAM. In this paper focused on the preparation of the DT bilayer, we did not investigate at length the exact nature of the Ag layer formed, which will be addressed in forthcoming work. A similar decrease was also observed for the BDMT-Ag case (fig.S4).

Upon re-immersion into BPD, one can observe notable changes in the $\delta\Psi$ and $\delta\Delta$ curves. The $\delta\Psi$ BPD-Ag-BPD curve shows a clear increase in magnitude below 600nm, related to an increase in the layer width. Correspondingly the $\delta\Delta$ curve is significantly more negative due to the much thicker BPD-Ag-BPD layer. A notable feature is the appearance of a more pronounced dip in the $\delta\Psi$, and $\delta\Delta$ curves, now at about 310nm. The change in the absorption at these wavelengths can be related to the formation of the longer molecule with four pyridine rings, which would lead to a shift of adsorption to longer wavelengths and decrease of the HOMO-LUMO gap.

When the procedure of adding first Ag and then BPD is continued in the same manner we observe a thickening of the layer, indicated by larger values $\delta\Psi$ and $\delta\Delta$ spectra as shown in fig.5 for BPD4. While we did not do any simulations, the almost double negative value of $\delta\Delta$ for BPD4 as compared with BPD2, is compatible with a doubling of the layer thickness. We also observe a further shift of the BPD4 adsorption to higher wavelengths: the main minimum is now at about 327nm. Thus these SE measurements indicate an initially rapid and then slower shift of the adsorption minimum to longer wavelengths when going from BPD1 to BPD2 and then to BPD4, which can be correlated to a decrease of the HOMO-LUMO gap in these systems, which varies here from about 4.51eV (BPD1) to 4eV (BPD2) and then to 3.8eV (BPD4).

Conductance measurements.

The length dependence of the conductance in molecular junctions is an interesting and important feature in molecular electronics and has been the object of a number of experimental and theoretical works.³⁷⁻⁴¹ We therefore investigated the

conductivity behavior for our BPD layers. To obtain reliable measurements of transport properties, it is common to use the mercury or EGaIn (gallium and indium alloy) drop method.^{37, 38} We established more than 20 junctions on each SAM configuration using the EGaIn drop as a top electrode.

Figure 6a shows the J-V curves for BPD1, BPD2, BPD3, and BPD4 layers. The curves are averages over 20 measurements and the vertical bar for BPD2 represents the typical scatter of these J-V curve data. Increase in length by forming multilayers can be seen to lead to a decrease in the conductivity. To check the effect of adding Ag, the J-V curve was measured for the BPD-Ag system and is also shown, with a vertical bar representing the typical scatter of data. It essentially coincides with that of the BPD1 curve, indicating that the Ag layer has no effect, as one would expect for metallic behavior, in agreement with the comment made in the XPS section above.

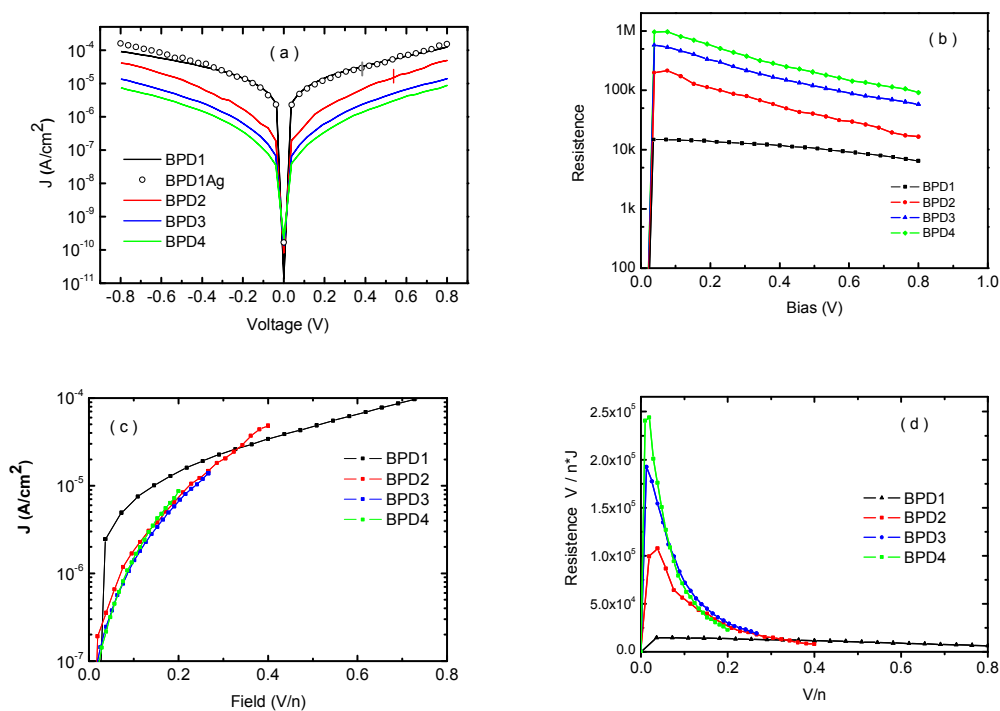


Figure 6: (a,b) Plot of current density and resistance as a function of the bias voltage and field (V/n) of four different molecular layers grown on gold, from the BPD1 to BPD4. (c,d) Plot of current density and resistance as a function of the field or bias across a single BPD unit.

In this figure one can see, that with increasing length the conductivity drops, and also that it drops faster in the beginning ie when going from BPD1 to BPD2. The decrease is then slower. This can also be seen in relative changes in the resistance (R) plot as a function of bias in fig.6b. This plot also shows that the bias dependence for BPD1 is quite different from that of the longer chains. One finds that the rate of decrease of resistance with bias is almost identical for BPD2 to BPD4, while it is significantly slower for BPD1 (see fig. S5 in supplementary information).

Rather than plotting J and R versus V, it was interesting to plot it as a function of V/n, where n is the number of BPD units, ie the field or bias across one BPD unit. These plots are shown in fig 6c and d. One can again we see a striking difference between BPD1 and BPD2 –BPD4, with a convergence for the case of BPD3 and BPD4. This convergence is particularly obvious for higher bias.

These data and plots clearly show a strong difference in behavior of conductance when going from the single BPD molecule to the longer chains.

Analysis of XPS and conductance data.

In the following we discuss briefly some aspects of the XPS data and look more closely at the conductance properties of the BPD and BPD_{Ag}BPD layers.

Characteristics of the XPS spectra.

The data presented above clearly shows that our approach leads to the formation of DT-Ag-DT nano-architected layers. We shall take a more detailed look at the XPS spectral shapes and intensities of the mono and bilayers in this context.

The shape evolution of the S2p spectra can be analyzed in more detail as follows. As in the previous work^{20, 23, 24} we assume that the intensity of electrons (A) passing through the standing up SAM is attenuated exponentially with thickness following the expression:

$$A/A_0 = \exp(-d/\lambda) \quad (1)$$

where A₀ is the initial intensity, d the organic layer thickness and λ the attenuation length. We assume an attenuation length of λ=2.5nm²⁰ and thickness d of 1.95nm, for the BPD SAM, as mentioned in the XPS section above.

This gives an attenuation of electrons from S adsorbed on Au (S_{Au}) by a factor of 0.46 for BPD, which corresponds fairly well with the lesser intensity of the S_{Au} peak in the figure 2a. The shape of the S(2p) spectrum will then be as indicated in fig. 7 (green triangles), which is the sum of contributions from S_{Au} and non-attenuated emission from the top S_H atoms.

As may be seen from experiment the proportion of the component corresponding to “free” S decreases after immersion in the Ag solution, while that corresponding to S_{Au} increases. However one can estimate that there remains a free S fraction of about 20%.

When the BPD-Ag SAM is immersed again into the BPD n-hexane solution, the spectrum changes and the “free” S_H atom contribution re-increases due to the BPD in solution binding to the top Ag atoms. To calculate the shape of the corresponding spectrum we assume that:

- S_{Au} intensity is attenuated by a 4,1nm thickness layer i.e. by a factor of 0.19
- S_H top has no attenuation
- S_{Ag} in the middle : for the now two S atoms, attenuation by a 1,95 nm top SAM with a 0.46 factor (assuming approximately the same attenuation for both atoms)

In case of a full coverage of the original BPD SAM by Ag we would then obtain a spectrum shown in fig 7 by the blue dots along with its constituent spectra for S_{Au} and S_H (blue lines). In case of 20% residual non Ag covered SAM and allowing for a small fraction (10%) of oxidized top S atoms, the resulting spectrum is shown in fig. 7 with red dots along with its constituent S_{Au} and S_H spectra (red crosses). Thus qualitatively the main changes in the XPS spectra and alternating changes in S_H peak intensity can be followed in this manner.

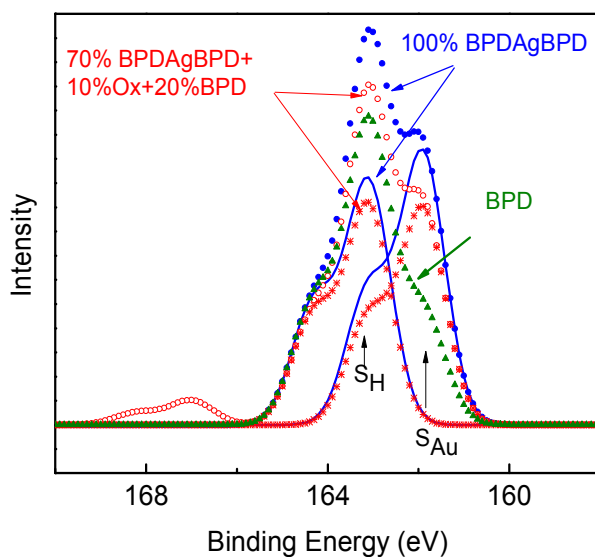


Figure 7. $S(2p)$ spectra for BPD (green triangles) and BPD_{Ag}BPD (full blue and empty red dots) simulated as described in the text.

The Ag3d intensity in fig 3 decreases after BPD adsorption by a factor of 0.5. This is in reasonable agreement with the 0.46 attenuation factor mentioned above for the BPD SAM.

One can similarly analyze the changes in the nitrogen signal intensity. Assuming for simplicity that the two N atoms are located at half the height of the BPD layer and using the 2,7nm attenuation length for Ag we can deduce the effective thickness of the Ag layer. It is then found to be about 0,7 nm, from the ratio of intensities of the N peak in the BPD (0.8) and BPD-Ag film (0.61). The latter intensities correspond to the normalization of the experimental BPD-Ag-BPD layer N peak to unity. The final intensity of the N peak can then be approximately calculated as given by the intensity of the N peak in the outer BPD layer, plus the intensity of the N peak in the BPD-Ag underlayer layer, which is attenuated by 0.46 (due to the BPD overlayer). This estimate gives an intensity of the N peak for the BPD-Ag-BPD layer as 1.1, which is reasonably close to the unit intensity in the experiment, given the approximations in this evaluation.

J-V measurements

In the preceding section we saw that there is a strong difference in behavior of conductance when going from the single BPD molecule to the longer chains and

differences as a function of bias are also observed. Following other works³⁷⁻⁴² we present this data in additional ways to further delineate some differences.

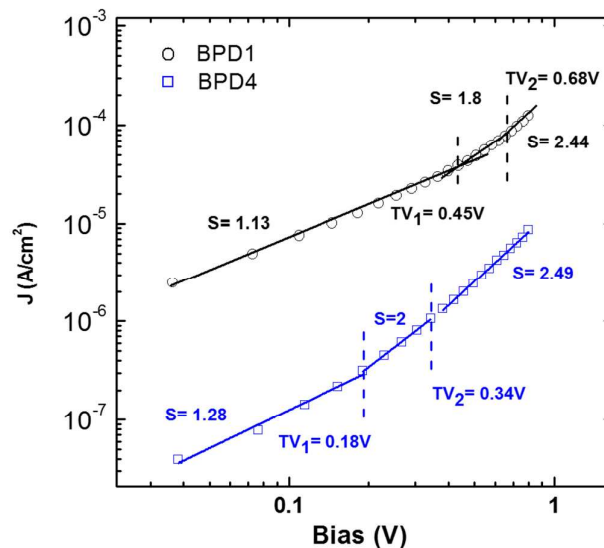


Figure 8. Log-log plot of the average J-V traces for the BPD and BPD4 junction. Fits are shown in different transport regimes.

Figure 8 shows the log (J)-log (V) plot of the J-V characteristics of the BPD1 and BPD4 systems between 0 and 0.8V. It is possible to discern different transport regimes as a function of the voltage. The BPD1 SAM reveals three distinct regimes. At the low voltage bias the plots are linear with a slope of about 1.13. Between 0.45 V and 0.68 V the BPD1 SAM exhibits a second, transition, regime with slope of about 1.18, while at higher bias the slope is 2.44. At the low voltage bias the BPD4 architecture shows a linear plot with a slope of about 1.28. The transition regime occurs between \sim 0.2 and 0.35 V. At the higher bias the plots are linear with a slope of about 2.49.

We have furthermore analyzed the Fowler-Nordheim (FN) type plot of BPD1 and BPD4 presented in figure 9 a, b (for other systems the plots are given in fig. S6). The FN type plot of $\ln(I/V^2)$ versus I/V for these systems shows the existence of three conduction regimes, with some similarities and differences.

For BPD at low bias one, we observe that J/V scales logarithmically with $1/V$ with a positive slope (see fig. 9-a). For low bias this behavior is compatible with a direct tunneling regime⁴², where the current is given by Eq. 2

$$\ln\left(\frac{J}{V^2}\right) \propto \ln\left(\frac{1}{V}\right) - \frac{2d}{\hbar} \sqrt{2m\phi} \quad (2)$$

Where d is the molecular length, m is the electron effective mass, and ϕ is the effective barrier height.

For BPD4 at low bias there is a different, linear dependence on $1/V$. At high bias both for BPD and BPD4 we observe a negative slope, which is considered to be characteristic of field emission⁴² and an intermediate transition regime. Here the linear scaling in both the above cases, with $1/V$, with a negative slope is characteristic of Fowler-Nordheim (FN) field driven conduction, where the current is given by Eq. 3

$$\ln\left(\frac{J}{V^2}\right) \propto \left(-\frac{4d\sqrt{2m}}{3q\hbar} \phi^{3/2}\right) \left(\frac{1}{V}\right) \quad (3)$$

The overall behavior of these systems in fig 8 and 9, is similar to recent reports of e.g. Choi et al⁴² for length dependence in conjugated molecular systems of increasing length, who concluded that they observe a transition from resonant tunneling to hopping at low bias when going from the shorter to longer molecules. In our case our data clearly shows a difference when going from BPD1 to the longer BPD2-4 systems, probably related to a similar change in conduction regime. At high bias in both cases the negative slope suggests field emission.

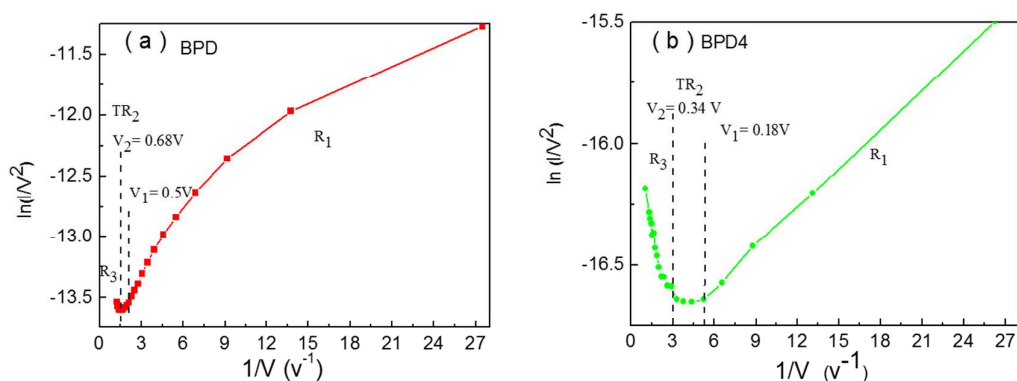


Figure 9. Fowler-Nordheim plot for the (a) BPD and (b) BPD4 data. Three distinct regimes (R_1 , TR_2 , and R_3) are evident.

It is generally considered, that when transport occurs via a tunneling process, the conductance (C) of molecular wires, decreases exponentially with increasing length³⁷⁻⁴³ l (see in particular the calculations and discussion in the recent paper of eg Peng et.al.⁴³)

$$C = I_0 e^{-\beta l}$$

where l is the length of the wire, C_0 is the contact conductance, which depends on the anchoring group, while the attenuation factor β depends on the characteristics of the molecules such as the HOMO-LUMO gap, molecular conformation, etc and apparently also to some extent on the anchoring group.⁴³

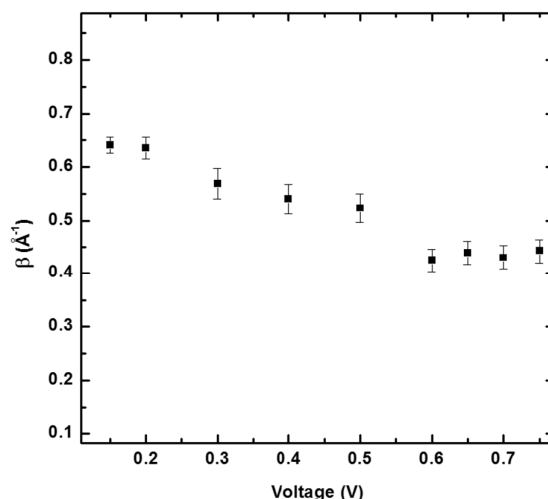


Figure 10: Plot of decay constant β for different values of the bias.

We calculated β values from our data in fig.6. As shown in fig 10, we find that β values exhibit three different plateaus as a function of the bias. From fig.10 an average $\beta_{\text{low bias}}$ of 0.64 \AA^{-1} can be calculated at the low bias range ($V < 0.3 \text{ V}$), β in the second plateau between 0.3 and 0.5 V has an average value of 0.54 \AA^{-1} , and at high bias $V > 0.5 \text{ V}$ $\beta_{\text{high bias}} = 0.45 \text{ \AA}^{-1}$. The β values from 0.64 \AA^{-1} to 0.45 \AA^{-1} in the applied bias range (0 to 0.8) are quite reasonable and agree well with the literatures.³⁷⁻⁴³

Theoretical calculations were performed on the following isolated molecules: (a) BPD, (b) BPD-Ag-BPD (BPD2), (c) and BPD-Ag-BPD-Ag-BPD (BPD3). See figure 1. Geometries, energies, and the changes in the electronic structure of the systems BPD, BPD2, BPD3 were obtained using a DFT calculation. The calculations were conducted using ORCA.⁴⁴ The PBE0⁴⁵ were used in combination with triple- ξ plus polarization basis set [Ahlich's TZV (2df, 2pd)].⁴⁶ the same correction factor has been added to calibrate the band gaps (band gap underestimation by DFT).

Figure 11 shows the density of the state of the BPD, BPD2, and the BPD3. We can see clearly that the HOMO-LUMO band gap decreases with increasing the number of layers. These calculations are in good agreement with spectroscopic ellipsometry observations, where the absorption maximum moves to longer wavelength as the number of the BPD layer increase. The general trend is consistent with earlier calculations on chains of some conjugated dithiol molecules.⁴³

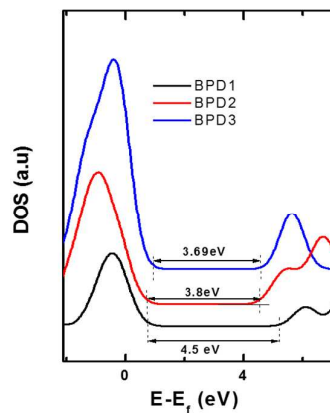


Figure 11: The density of the state DOS at the valence band for the BPD1, BPD2, BPD3

The transition energy (V_T) determined from the slope of the $I-V$ characteristics and the *Fowler-Nordheim* plot for the different BPD layers, shows decrease in V_T with increase of the number of layers. This variation can be attributed to the changes in the electronic structure of the system, where the decrease in the band gap value is accompanied by an important degree of electron delocalization in the system.

Conclusion

This work thus clearly shows that using an appropriate and robust protocol for dithiol SAM formation, developed by us previously, an organic molecule metal multilayer scaffold can be nano-architected, whose characteristics can be tuned by adjusting the number of layers.

These layers exhibit some interesting characteristics, such as the absorption features in the 350nm-500nm region ascribable to the existence of the intercalated Ag and which with further work could possibly be exploited in a plasmonic application.

We also see absorption in the 250nm to 350nm region is observed which is ascribable to benzene and pyridine and we observe a shift in the absorption feature to higher wavelengths, which can be ascribed to changes in HOMO-LUMO splitting, which were reproduced in DFT calculations.

From the point of view of molecular conductance, this system exhibits interesting changes in the J - V characteristics when the number of layers is progressively increased, going from mono to multilayers. More detailed theoretical studies on transport are necessary to better understand conductance in these systems. On the experimental side temperature dependence studies are also required, which were not possible here with the EGaIn drop electrode.

The procedure of DT-Ag-DT preparation we outline, could be useful in applications involving molecular electronics, plasmonics and more complex metal organic hetrostructures. An improvement in methodology could involve vapor phase deposition of Ag atoms in high vacuum, which would minimize unwanted oxidation effects in aqueous medium.

Acknowledgements.

VAE thanks ICYS-MANA for supporting his stay at NIMS. We appreciate the valuable assistance of MANA foundry. This work has been supported by the International Center for Young Scientists (ICYS) on Materials Nanoarchitectonics (WPI –MANA).

References.

1. K. Rajalingam, T. Strunskus, A. Terfort, R. Fischer, C. Wöll, *Langmuir*, 2008, 24, 7986–7994
2. Angélique Bétard and Roland A. Fischer. *Chem. Rev.*, 2012, 112, 1055–1083
3. H. Rieley, G. K. Kendall, F.W. Zemicael, T. L. Smith, and S. Yang, *Langmuir* 1998, 14, 5147– 5153
4. K. V. Sarathy, P. J. Thomas, G. U. Kulkarni, and C. N. R. Rao, *J. Phys. Chem. B* 1999, 103, 399– 401
5. A. K. A. Aliganda, I. Lieberwirth, G. Glasser, Duwez,; A.-S. Sun, Y, S. Mittler, *Org. Electron.* 2007, 8, 161– 174
6. H. Hamoudi, *Nanoscale Res Lett*, 2014, 9:287 doi:10.1186/1556-276X-9-287
7. F, Chesneau. M, Zharnikov, *J. Phys. Chem. C*, 2014, 118, 12980–12988

8. W. Azzam, B. I. Wehner, R. A. Fischer, A. Terfort, C. Wöll, *Langmuir* 2002, 18, 7766–7769
9. Y. Tai, A. Shaporenko, H.-T. Rong, M. Buck, W. Eck, M. Grunze, M. Zharnikov, *J. Phys. Chem. B* 2004, 108, 16806–16810
10. Y. -C. Yang, Y.-L. Lee, L.-Y. Ou Yang, S.-L. Yau, *Langmuir* 2006, 22, 5189–5195
11. D. L. Pugmire, M. J. Tarlov, and R. D. Van Zee, *Langmuir* 2003, 19, 3720–3726
12. L. Pasquali, F. Terzi, C. Zanardi, L. Pigani, R. Seeber, G. Paolicelli, S. M. Sutturin, N. Mahne, and S. Nannarone, *Surf. Sci.* 2007, 601, 1419–1427
13. L. Pasquali, F. Terzi, R. Seeber, B. P. Doyle, and S. J. Nannarone, *Chem. Phys.* 2008, 128, 134711
14. S. W. Joo, S. W. Han, and K. Kim, *J. Phys. Chem. B* 1999, 103, 10831–10837
15. S. Rifai, and M. Morin, *J. Electroanal. Chem.* 2003, 550–551, 277–289
16. Ulrike Weckenmann, Silvia Mittler, Kai Naumann, and Roland A. Fischer
Langmuir, 2002, 18, 5479–5486
17. C. Silien, L. Dreesen, F. Cecchet, P. A. Thiry, and A. Peremans, *J. Phys. Chem. C* 2007, 111, 6357–6364
18. M. Venkataramanan, S. Ma, , and T. Pradeep, *J. Colloid Interface Sci.* 1999, 216, 134–142
19. R. P. Andres, T. Bein, M. Dorogi, S. Feng, J. I. Henderson, C. P. Kubiak, W. Mahoney, R. G. Osifchin, R. Reifengerger, *Science* 1996, 272, 1323–1325
20. H. Hamoudi, Z. A. Guo, M. Prato, C. Dablemont, W. Q. Zheng, B. Bourguignon, M. Canepa, V. A. Esaulov, *Phys. Chem. Chem. Phys.* 2008, 10, 6836–6841
21. Hamoudi, H.; Dablemont, C.; Esaulov, V. A. *Surf. Sci.* 2011, 605, 116
22. M. A. Daza Milone, H. Hamoudi, L. M. Rodríguez, A. Rubert, G. A. Benitez, M. E. Vela, R. C. Salvarezza, J. E. Gayone, E. A. Sánchez, O. Grizzi, C. Dablemont, V. A. Esaulov, *Langmuir* 2009, 25, 12945–12953
23. H. Hamoudi, M. Prato, C. Dablemont, O. Cavalleri, M. Canepa, V. A. Esaulov, *Langmuir* 2010, 26, 7242–7247
24. Luca Pasquali, Fabio Terzi, Renato Seeber, Stefano Nannarone, Debasish Datta, Céline Dablemont, Hicham Hamoudi, Maurizio Canepa, Vladimir A Esaulov
Langmuir 27, 2011, 4713-4720

25. J. Jia, S. Mukherjee, H. Hamoudi, S. Nannarone, L. Pasquali, V. A. Esaulov
The Journal of Physical Chemistry C 117, 2013, 4625-4631
26. L. Salazar Alarcón, L. J. Cristina, J. Shen, J. Jia, V. A. Esaulov, E. A. Sánchez, O. Grizzi, *The Journal of Physical Chemistry C* 117, 2013, 17521-17530
27. L. S. Alarcón, L. Chen, V. A. Esaulov, J. E. Gayone, E. A. Sánchez, O. Grizzi
The Journal of Physical Chemistry C 2010, 114, 19993-19999
28. M. Canepa, G. Maidecchi, T. Chiara, O. Cavalleri, M. Prato, V. R. Chaudhari, V. A. Esaulov. *Phys. Chem. Chem. Phys.* 2013, **15**, 11559-11565
29. Maurizio Canepa, *Surface Science Techniques*. G. Bracco, B. Holst. *Springer Series in Surface Sciences* (2013). 99,135
30. M. Prato, R. Moroni, F. Bisio, R. Rolandi, L. Mattera, O. Cavalleri and M. Canepa,
J. Phys. Chem. C, 2008, 112, 3899–3906
31. H. Hamoudi, K. Döring, F. Chesneau, H. Lang, M. Zharnikov. *J. Phys. Chem. C*.
2011, 116, 861-870
32. Juanjuan Jia, Azzedine Bendounan, Harish Makri Nimbegondi Kotresh, Karine Chaouchi, Fausto Sirotti, Srinivasan Sampath, and Vladimir A. Esaulov, *J. Phys. Chem. C*, 2013, 117 (19), pp 9835–9842
33. D. David. J. r. Evanoff, and George Chumanov, *J. Phys. Chem. B* 2004, 108, 13957-13962
34. David D. Evanoff Jr. and George Chumanov, *ChemPhysChem* 2005, 6, 1221 – 1231
35. W. Schulze, H.U. Becker and H. Abe , *Chemical Physics* 35 (! 978) 177-I 86
36. G. Agostini, S. Usseglio, E. Groppo, M. J. Uddin, C. Prestipino, S. Bordiga, A. Zecchina, P. L. Solari, and C. Lamberti ,*Chem. Mater.* **2009**, 21, 1343–1353
37. D. M. Adams, L. Brus, C. E. D. Chidsey, S. Creager, C. Creutz, Kagan, C. R. P. V. Kamat, M. Lieberman, S. Lindsay, R. A. Marcus, et al. *J. Phys. Chem. B* 2003, 107, 6668–6697.
38. R. E. Holmlin, R. Haag, R. F. Ismagilov, M. A. Rampi, G. M. Whitesides, *J. Am. Chem. Soc.* 2001, 123, 5075.
39. D. J. Wold, R. Haag, M. A. Rampi, C. D. Frisbie, *J. Phys. Chem. B* 2002, 106, 2813–2816.
40. A. V. Tivanski, Y. He, E. Borguet, H. Liu, G. C. Walker, D. H. Waldeck, *J. Phys. Chem. B* 2005, 109, 5398–4502.

41. C. Musumeci, G. Zappala, N. Martsinovich, E. Orgiu, S. Schuster, S. Quici, M. Zharnikov, A. Troisi, A. Licciardello and P. Samori *Adv. Mater.* 26, 1688–1693 (2014)
Adv. Mater. 2014, 26, 1688–1693
42. Seong Ho Choi, BongSoo Kim, C. Daniel Frisbie. *Science*. 2008, 320, 1482
43. Guowen Peng, Mikkel Strange, Kristian S. Thygesen, and Manos Mavrikakis, *J. Phys. Chem. C* **2009**, 113, 20967–20973
44. Neese F ORCA: an *ab initio* DFT and semiempirical SCF-MO package, University of Bonn, Bonn, Germany, **2007**.
45. C. Adamo, V. J. Barone: *Chem. Phys.* **1999**, 110, 6158–6170.
46. A. Schafer. H, Horn. R. Ahlrichs, *J. Chem. Phys.* **1992**, 97, 2571–2577.
47. Qu, D. and Uosaki, K. *J. Phys. Chem. B* 2006, 110, 17570– 17577
48. K, Rajalingam. T, Strunskus. A, Terfort. R. A. Fischer. C, Wöll. *Langmuir*, 2008, 24, 7986–7994
49. D. Qu, and K. Uosaki, *J. Phys. Chem. B* 2006, 110, 17570– 17577
50. H, Hamoudi, *RSC Advances*, 2014, 4 , 22035-22041
51. A. DiBenedetto, A. Facchetti, M, A, Ratner. T, J, Marks. *Adv. Mater.* 2009, 21, 1407–1433,
52. C, I, Drexler. K, B, Moore. C, P, Causey. T, J, Mullen, *Langmuir*, 2014, 30 (25), pp 7447–7455,
53. Markus Holzweber, Thomas Heinrich, Valentin Kunz, Sebastian Richter, Christoph H.-H. Traulsen, Christoph A. Schalley, and Wolfgang E. S. Unger, *Anal. Chem.* 2014, 86 (12), pp 5740–5748,
54. H, K, Arslan. O, Shekhah. D, C, F, Wieland. M, Paulus. C, Sternemann. M, A, Schroer. S, Tiemeyer. M, Tolan. R, A, Fischer. C, Wöll , *J. Am. Chem. Soc.*, 2011, 133, 8158–8161